SUMOylation of $Na_V1.2$ channels regulates the velocity of backpropagating action potentials in cortical pyramidal neurons

Authors: Oron Kotler,[1] Yana Khrapunsky,[1] Arik Shvartsman[1], Hui Dai,[2] Leigh D. Plant,[3] Steven A.N. Goldstein,[2*] and Ilya Fleidervish[1*]

* Co-corresponding authors

[1] Department of Physiology and Cell Biology, Faculty of Health Sciences, Ben-Gurion University of the Negev, Beer Sheva 84105, Israel

[2] Departments of Pediatrics and Physiology & Biophysics, University of California, Irvine, 1001 Health Sciences Road, Irvine Hall, Irvine, CA 92697, USA

[3] Department of Pharmaceutical Sciences, Northeastern University, 360 Huntington Avenue, Boston, MA 02115, USA

Corresponding Authors: Ilya Fleidervish & Steven A.N. Goldstein

Emails: ilya@bgu.ac.il (I.F.), sgoldst2@hs.uci.edu (S.G.)

Keywords: axon initial segment, layer 5 pyramidal neurons, $Na_v1.2$, SUMO, SENP, action potential, backpropagation, I_{NaP}, neuronal excitability

This file includes:

Abstract

Voltage-gated sodium channels located in axon initial segments (AIS) trigger action potentials (AP) and play pivotal roles in the excitability of cortical pyramidal neurons. The differential electrophysiological properties and distributions of $Na_V1.2$ and $Na_V1.6$ channels lead to distinct contributions to AP initiation and backpropagation. While $Na_V1.6$ at the distal AIS promotes AP initiation and forward propagation, $Na_V1.2$ at the proximal AIS promotes backpropagation of APs to the soma. Here, we show the Small Ubiquitin-like Modifier (SUMO) pathway modulates persistent sodium current (I_{NaP}) generation at the AIS to increase neuronal gain and the speed of backpropagation. Since SUMO does not affect $Na_V1.6$, these effects were attributed to SUMOylation of $Na_V1.2$. Moreover, SUMO effects were absent in a mouse engineered to express $Na_V1.2$-Lys38Gln channels that lack the site for SUMO linkage. Thus, SUMOylation of $Na_V1.2$ exclusively controls I_{NaP} generation and AP backpropagation, thereby playing a prominent role in synaptic integration and plasticity.

Significance Statement

Resolving a long-standing controversy, SUMOylation of $Na_V1.2$ channels is revealed to regulate the excitability of cortical neurons by augmenting persistent sodium current at critical subthreshold voltages. SUMOylation increases the speed of action potential backpropagation from the axon initial segment to the soma, a phenomenon critical to long-term potentiation, spike-time dependent plasticity, and release of retrograde factors essential to synaptic plasticity and development.

Main Text

Introduction

In cortical pyramidal cells, as in many CNS neurons, action potentials (APs) initiate in the axon initial segment (AIS), the proximal part of the axon where the neuronal membrane is not covered with a myelin sheath. The AIS is characterized by specialized assembly of scaffolding proteins and voltage-gated channels with distinctive biophysical properties (Bean, 2007; Rasband, 2010). Classically, APs propagate forward from the AIS into the axonal arbor where they trigger neurotransmitter release from presynaptic terminals. APs can also propagate backward into the dendrites of cortical pyramidal cells where they are proposed to play a role in synaptic plasticity by regulating synaptic strength and the coordination of synaptic inputs (Stuart and Sakmann, 1994; Markram et al., 1997). Both the initiation and propagation of APs are critically dependent on the distribution and properties of voltage-gated Na^+ (Na_V) channels in specific neuronal compartments (Stuart et al., 1997; Hu et al., 2009; Baranauskas et al., 2013). Therefore, identifying signaling pathways that regulate the biophysical properties of neuronal Na_V channels is key to understanding spike generation, propagation and integration in cortical circuits (Cantrell et al., 1996; Cantrell and Catterall, 2001; Bender et al., 2012; Kole and Stuart, 2012; Yin et al., 2017).

Central neurons express, to varying degrees, three primary Na_V channels α-subunit isoforms. $Na_V1.1$, $Na_V1.2$, and $Na_V1.6$ are found in mature neurons while $Na_V1.3$ channels also found in the developing nervous system (Goldin et al., 2000). Each Na_V isoform has a distinct spatiotemporal distribution and is subject to the activity of specific signaling pathways that regulate the biophysical properties and trafficking behavior of the

channel. For example, in mature pyramidal neurons, the AP trigger zone, which is located in the distal AIS, contains almost exclusively $Na_V1.6$ channels (Lorincz and Nusser, 2008; Hu et al., 2009; Lorincz and Nusser, 2010; Tian et al., 2014). These channels are also present in the nodes of Ranvier (Caldwell et al., 2000). In contrast, the proximal portion of the AIS, soma and dendrites are believed to contain mostly $Na_V1.2$ channels (Hu et al., 2009; Grubb et al., 2011). While this difference in distribution has long made it tempting to posit that the initiation and forward propagation of APs are predominately dependent on $Na_V1.6$ channels and the backpropagation of APs is dependent on the activity of $Na_V1.2$ channels, studies of the biophysical attributes of the two channels have not previously verified this hypothesis.

While heterologous studies show that $Na_V1.6$ channels activate at more negative voltages than other neuronal Na_V isoforms and have a higher propensity to generate non-inactivating currents, differences in the gating behavior of $Na_V1.2$ and $Na_V1.6$ channels appear to be subtle within their native neuronal milieu (Smith et al., 1998; Zhou and Goldin, 2004; Rush et al., 2005; Chen et al., 2008). Indeed, using knockout mice, we found that $Na_V1.6$ channels were not required to determine the initiation site for APs within the AIS, for backpropagation into the dendrites, or for the lower activation threshold voltage for APs that is commonly observed in pyramidal neurons (Katz et al., 2018).

Although the biophysical differences between native $Na_V1.2$ and $Na_V1.6$ are subtle, each channel isoform is differentially regulated by neuromodulators. Thus, $Na_V1.6$ channels are less sensitive to inhibition by cAMP-dependent protein kinase or protein kinase C mediated phosphorylation (Chen et al., 2008). This finding explains

100 divergent regulation of Na_V channel subtypes following the activation of D1/D5
101 dopamine or 5-HT_{1A} serotonergic receptors (Maurice et al., 2001; Yin et al., 2017). We
102 have shown that ion channels are also subject to post-translational regulation by covalent
103 linkage of Small Ubiquitin-like Modifier (SUMO) proteins (Rajan et al., 2005; Plant et al.,
104 2010; Plant et al., 2011; Plant et al., 2012; Plant et al., 2016; Xiong et al., 2017; Plant et
105 al., 2020). Three SUMO isoforms (SUMO1-3) are operative in central neurons and can
106 modulate the gating of specific channels following their conjugation to the ε-amino group
107 of specific lysine residues on the intracellular termini or cytoplasmic loops of the channel
108 subunits. Further, we found the enzymes required to activate, mature and conjugate
109 SUMO reside in the plasma membrane of *Xenopus* oocytes, tissue culture cells and
110 neurons (Rajan et al., 2005; Plant et al., 2010; Plant et al., 2011; Plant et al., 2016).
111 Although SUMOylation is a covalent post-translational modification it is a dynamic
112 process subject to rapid reversal by the action of the SENP family of sentrin-specific
113 cysteine proteases. Thus far, we have observed that SUMOylation increases excitability
114 either by decreasing potassium flux through K_V and K2P channels or by increasing the
115 activity of Na_V channels and that the opposite functional effects are mediated by the
116 activity of SENPs. Further, we have shown that SUMO has differential effects on the
117 principal Na_V channel isoforms expressed in central neurons. Specifically, we found that
118 SUMOylation modulates the voltage-dependent gating of $Na_V1.2$ channels via linking to
119 Lysine 38, but SUMO does not interact with $Na_V1.6$ (Plant et al., 2016).

120 Here, we tested the hypothesis that SUMOylation regulates the excitability of
121 cortical pyramidal neurons. By combining whole-cell recordings with high-speed
122 fluorescence imaging to simultaneously monitor Na^+ flux in different subcellular

123 compartments of L5 cortical neurons we found that SUMO1 increases excitability via a
124 synergistic effect on subthreshold K^+ and Na^+ conductances. Thus, SUMOylation
125 suppresses the open probability of K^+ channels, while concurrently increasing Na^+ influx
126 via a leftward shift in the steady-state activation of subthreshold persistent Na^+ currents.
127 These effects are absent in a CRISPR-generated mouse that constitutively expresses
128 $Na_V1.2$-Lys38Gln channels, a channel variant that cannot be SUMOylated. Confirming
129 the long-held notion for their roles in the AIS based on distribution, and consistent with
130 our previous report that SUMO regulates $Na_V1.2$ but not $Na_V1.6$ channels, we
131 demonstrate that SUMOylation of $Na_V1.2$ regulates the velocity of backpropagation in
132 cortical pyramidal neurons independent of the speed at which AP propagate forward from
133 the AIS.

134

135 **Results**

136 **SUMO1 increases the excitability of layer 5 cortical neurons**

137 Previously, we showed that the effects of SUMOylation and deSUMOylation of neuronal
138 ion channels underlying I_{DR}, $I_{Kso,}$ and I_{Na} could be assessed by including purified SUMO1
139 or SENP1 peptides, respectively, in the recording pipette solution (Plant et al., 2011;
140 Plant et al., 2012; Plant et al., 2016). To characterize the effects of the SUMO pathway
141 on the excitability of layer 5 cortical pyramidal neurons, we made whole-cell, current-
142 clamp recordings from these cells using pipettes filled with a solution containing SUMO1
143 or SENP1 peptides at 1000 and 250 pmol/L, respectively. We have previously shown
144 that peptides at these concentrations produce maximal effects on K_V, $K_{2P,}$ and Na_V

145 channels in cultured rat hippocampal neurons, cerebellar granule neurons, human
146 ventricular cardiomyocytes derived from iPS cells, and on channels expressed in
147 heterologous cell systems (Plant et al., 2010; Plant et al., 2011; Plant et al., 2012; Plant et
148 al., 2016; Plant et al., 2020).

149 Passive neuronal properties and repetitive firing characteristics were assessed by
150 examining the voltage responses to a series of prolonged hyperpolarizing and
151 depolarizing current pulses delivered via the somatic pipette. Because cortical cells are
152 geometrically complex, we compared data obtained two minutes and 35 minutes after
153 break-through into whole-cell configuration to account for slow intracellular dialysis of
154 the peptide into the neurons. As SUMO1 diffused into the cell, the frequency of spike
155 firing in response to a given depolarizing suprathreshold current pulse increased (**Figure**
156 **1a**). Thus, the mean instantaneous firing frequency in response to a 0.3 nA current
157 injection increased from 14.7±3.9 Hz immediately after the break-in to 25.7±5.4 Hz (n=6,
158 p=0.029) after 35 mins of SUMO1 dialysis. In contrast, dialysis with the SENP1-
159 containing solution caused a gradual decrease in the frequency of repetitive firing over
160 time. The mean instantaneous firing frequency in response to a 0.3 nA current pulse
161 decreased from 15.6±2.3 Hz immediately after the break-in to 5.3±1.8 Hz (n=5, p=0.004)
162 after 35 mins of SENP1 dialysis.

163 Examining the voltage responses to small hyperpolarizing current pulses before
164 and following the SUMO1 and SENP1 dialysis revealed that the peptides elicited
165 opposite effects on passive neuronal properties (**Figure 1b**). Thus, the apparent input
166 resistance (R_{in}), calculated as a ratio of the steady-state amplitude of the voltage
167 deflection to current amplitude, gradually increased when SUMO1 was included in the

pipette, from 96.8 ± 12.9 MΩ at a time of break-in to the cell to 120.7 ± 14.5 MΩ (n=6, $p<0.03$) at 35 min of recording. In contrast, dialysis of the neurons with SENP1 caused R_{in} to decrease as a function of recording time from 119.4 ± 13.6 MΩ to 82.2 ± 5.4 MΩ (n=5, $p<0.02$). In parallel, the membrane time constant (τ_m) obtained by fitting a mono-exponential function to the voltage transient following the end of the hyperpolarizing current pulse, was increased by SUMO1 application from 14.4 ±1.9 ms at the time of break-in to 19.1 ±3.2 ms (n=6, $p<0.03$) and shortened by SENP1 application from 19.5 ±2.34 ms to 14.1 ± 2.3 ms (n=5, $p<0.02$). Recording of similar duration with control intracellular solution had no significant effect on R_{in} (112.8 ± 19.1 vs. 113.1 ± 18.2 MΩ, n=5, $p=0.83$) and τ_m (14.8 ± 1.1 vs. 15.2 ± 1.2 ms, n=5, $p=0.13$). These findings indicate that in L5 cortical neurons the SUMO pathway regulates potassium channels that determine the passive membrane properties. Furthermore, the relatively high effectiveness of SENP1 suggests that in L5 neurons, as in other cell types (Rajan et al., 2005; Plant et al., 2011; Plant et al., 2012; Plant et al., 2016; Xiong et al., 2017), a significant fraction of these channels are SUMOylated under control conditions.

The effect of SUMO1 and SENP1 on repetitive firing may reflect the action of the peptides on passive neuronal characteristics or their influence on the ion currents underlying spike generation. Theoretical analysis revealed that while the former mechanism should elicit a parallel shift of the frequency–current (F-I) curve to the right or left along the current axis (Chance et al., 2002), the latter should alter the neuronal gain, i.e., the steepness of the slope of the F-I characteristic. Comparing the linear fits of the mean F-I curves obtained immediately after the break-in and following the SUMO1 dialysis, we found that the curve steepness increased by ~75%, from 60 to 106 Hz/ nA (n

= 6) (**Figure 1 – Figure Supplement 1**). Dialysis with control pipette solution had little to no effect on the neuronal gain (63 vs. 78 Hz/nA, respectively, n=5). In contrast, in recordings with SENP1 containing pipette, the gain decreased from 98 to 33 Hz/ nA (n = 5).

To test our hypothesis that SUMOylation of $Na_V1.2$ channels can regulate the excitability of L5 cortical neurons, we used CRISPR/ Cas9 to engineer a mouse model carrying $Na_V1.2$-Lys38Gln, a mutation that removes the only SUMO-conjugation site in $Na_V1.2$ channels (Plant et al., 2016). The genotype of the mice was verified by PCR screening and sequencing analysis (**Supplementary Figure S1**). First, we sought to find out whether SUMO1 and SENP1 dialysis affect the F-I relationship of L5 neurons from the $Na_V1.2$-Lys38Gln mutant mice (**Figure 2a**). As in WT neurons, SUMO1 dialysis enhanced the frequency of repetitive firing for a given amplitude of the current pulse, whereas the SENP1 dialysis had the opposite effect. Thus, the mean instantaneous firing frequency in response to a 0.3 nA current injection increased from 18.3±2.0 Hz immediately after the break-in to 21.4±1.7 Hz (n=10, p=0.017) after 35 mins of SUMO1 dialysis. In contrast, the mean instantaneous firing frequency decreased from 20.7±3.1 Hz immediately after the break-in to 11.5±5.9 Hz (n=7, p=0.035) after 35 mins of SENP1 dialysis.

Both treatments, however, affected the position of the F-I curve relative to the current axis while little to no effect on its slope was observed (**Figure 2b**), consistent with the hypothesis that, in $Na_V1.2$-Lys38Gln neurons, SUMOylation primarily affects passive neuronal properties. Indeed, in $Na_V1.2$-Lys38Gln mutant neurons, SUMO1 dialysis increased the apparent R_{in} (from 131.9 ± 17.9 MΩ to 161.3 ± 20.1 MΩ, n=7,

214 p<0.003) whereas dialysis with SENP1 had an opposite effect (from 170.5 ± 13.2 MΩ to
215 92.7 ± 12.4 MΩ, n=6, p<0.005) (**Figure 2c**).

216

217 **SUMO1 and SENP1 have the opposite effect on the voltage-dependence of I_{NaP}**

218 In cortical pyramidal neurons, the persistent sodium current operates at a
219 subthreshold range of voltages and is one of the main factors influencing the frequency of
220 repetitive firing, thereby modifying the neuronal gain (Stuart and Sakmann, 1995;
221 Astman et al., 2006). We have recently shown that in pyramidal cells, most I_{NaP} is
222 generated by somatodendritic Na^+ channels (Fleidervish et al., 2010; Shvartsman et al.,
223 2021). The immunohistochemical evidence indicates that soma, dendrites, and proximal
224 AIS of L5 pyramidal neurons are populated predominately by the $Na_V1.2$ channels whose
225 activation and inactivation gating is sensitive to SUMOylation (Hu et al., 2009; Grubb et
226 al., 2011; Plant et al., 2016). In contrast, the membrane of the distal AIS and the nodes of
227 Ranvier contains $Na_V1.6$ channels which lack SUMO binding domain (Plant et al., 2016).
228 In order to find out how SUMO1 and SENP1 affect the persistent sodium current in
229 different neuronal compartments, we combined whole-cell, voltage-clamp recordings
230 from L5 neurons with high-speed fluorescence imaging of a Na^+ sensitive dye, SBFI. A
231 comparison of the voltage ramp elicited Na^+ fluxes revealed that SUMO1 dialysis
232 induces a left shift in the I_{NaP} activation kinetics in soma, proximal apical dendrite, and in
233 the AIS of L5 neurons (**Figure 3a**). Thus, at a voltage of -50 mV, the relatively small
234 fluorescence change in the soma and apical dendrites was significantly increased by
235 SUMO1 dialysis, whereas the amplitude of the Na^+ signal in the AIS was less markedly
236 increased (**Figure 3b)**.

Measurements of half-activation voltage (V½) revealed that SUMO1 dialysis causes a significant leftward shift in the activation kinetics of both somatic channels and axonal channels in WT neurons (**Figure 3 – Figure Supplement 1**). However, the application of SUMO1 produced no effect on the voltage dependence of I_{NaP} in neurons from $Na_V1.2$-Lys38Gln mice (**Figure 3 – Figure Supplement 2**). Intracellular application of SENP1 resulted in an opposite effect on the voltage-dependence of I_{NaP}. Thus, a small but significant rightward shift in the V½ of I_{NaP} was observed in the soma and AIS of neurons from WT, but not $Na_V1.2$-Lys38Gln mice (**Figure 4**). These findings indicate that in cortical neurons a portion of the $Na_V1.2$ channels is SUMOylated under control conditions.

SUMOylation of Na^+ channels affects voltage-dependent amplification of EPSPs in pyramidal neurons

Changes in the amplitude of I_{NaP} at subthreshold voltages are expected to influence the spatial and temporal summation of synaptic potentials (Deisz et al., 1991; Stuart and Sakmann, 1995; Stuart, 1999). Therefore, we studied the effect of SUMOylation on the amplitude and duration of EPSPs elicited in the pyramidal neuron by brief synaptic stimuli. The EPSPs were measured immediately after break-in to the whole-cell configuration and following 30 minutes of intracellular dialysis with SUMO1 in WT and $Na_V1.2$-Lys38Gln neurons. SUMO1 did not change the duration of small EPSPs of less than 10 mV in amplitude (**Figure 5a**). In contrast, SUMO1 prolonged the decay time constant of EPSPs greater than 10 mV in amplitude in WT but not $Na_V1.2$-Lys38Gln neurons. In pooled EPSPs obtained from six neurons in each experimental group, SUMO1 dialysis enhanced the steepness of the slope of EPSP integral-to-peak

relationship (**Figure 5b**) in WT neurons, whereas SUMOylation had no effect on this relationship for $Na_V1.2$-Lys38Gln cells.

SUMOylation differentially affects the speed of forward- and back-propagating action potentials

In cortical pyramidal neurons, the $Na_V1.2$ channels are predominately localized in somatic, dendritic, and proximal AIS membrane where they are responsible for the propagation of action potentials back into the dendritic tree (Hu et al., 2009; Grubb et al., 2011). The $Na_V1.6$ channel subtype is present in the distal AIS and in the nodes of Ranvier and it is responsible for forward propagation of action potentials into the axonal arbor (Hu et al., 2009). Because $Na_V1.2$ and $Na_V1.6$ channels respond differentially to SUMOylation, with the former being susceptible and the latter resistant to SUMO1, we hypothesized that this neuromodulation could differentially affect the speed of forward and backpropagation of the spikes. Seeking to test this hypothesis directly, we measured the velocity of forward and backpropagation using paired, whole-cell, loose patch recordings to detect the times of the spike arrival from multiple sites along the axo-somatic axis in sequence (**Figure 6**) (Baranauskas et al., 2013; Lezmy et al., 2017). In order to distinguish the axon from other thin processes emerging from the cell body, and to facilitate the distance measurements between the somatic and axonal pipettes, we filled the neurons for at least 15 minutes with the Na^+-sensitive dye SBFI. Because of this and the relatively long time it takes to obtain action currents from multiple axonal locations, we were not able to measure the propagation velocity upon break-in to whole-cell configuration. Thus, we compared the propagation velocities in WT neurons dialyzed either with control or SUMO1 containing intracellular solution. As an additional control,

283 the same measurements were taken from the $Na_V1.2$-Lys38Gln neurons dialyzed with
284 SUMO1.

285 As demonstrated by a representative untreated WT cell (**Figure 6a**),
286 backpropagation velocity (0.10 m/s) was significantly lower than the velocity of forward
287 propagation (0.32 m/s). Dialysis with SUMO1, however, speeded the backpropagation,
288 such that its velocity became almost equal to the speed of forward propagation, ~0.27 vs.
289 0.23 m/s for forward and backpropagation, respectively (**Figure 6b**). This effect of
290 SUMO1 was not observed in $Na_V1.2$-Lys38Gln neurons, in which the backpropagation
291 was still significantly slower than forward propagation, ~0.26 vs. 0.12 m/s for forward
292 and backpropagation, respectively (**Figure 6c**). Comparison of the ratios of backward
293 and forward propagation velocities revealed a significant increase in WT neurons
294 dialyzed with SUMO1, as compared with untreated WT or SUMO1 treated $Na_V1.2$-
295 Lys38Gln cells (**Figure 6d**). To find out whether the leftward shift of $Na_V1.2$ activation
296 kinetics could increase the backpropagation velocity, we studied the dynamics of AP
297 propagation in a simplified compartmental model in which we distributed the $Na_V1.2$ and
298 $Na_V1.6$ channels in accordance with immunohistochemical data (Hu et al., 2009). In
299 good agreement with our experimental results, a 6 mV leftward shift in half-activation
300 voltage of $Na_V1.2$ caused an about two-fold increase in AP backpropagation velocity
301 (**Figure 6 – Figure Supplement 1**) whereas the forward propagation remained almost
302 unaffected. Thus, our data indicates that in cortical pyramidal neurons SUMOylation of
303 $Na_V1.2$ channels could provide a "switch" allowing differential regulation of the AP
304 invasion into the dendritic tree and synaptic plasticity whereas, the ongoing neuronal

activity that relies on SUMO-resistant, Nav1.6-mediated, spike forward propagation, would not be affected.

Discussion

We have shown before that SUMOylation has opposite but synergistic effects on Na^+ and K^+ channel gating that conspire to increase the excitability and demonstrate that role of the regulatory pathway here in cortical pyramidal neurons. On the one hand, SUMO1 increases the inward Na^+ current, and on the other hand, it decreases the outward potassium current at the sub-threshold range of voltages. Together, the SUMOylation of these channels modulates the gain of neuronal responses to depolarizing current injection by affecting the steepness of the post-spike voltage trajectory towards the next spike threshold. In contrast, deSUMOylation of Na^+ and K^+ channels by SENP1 decreased neuronal gain indicating that native neuronal channels are partially SUMOylated under baseline conditions. These findings are congruent with reports describing SUMO-regulation of Na^+ and K^+ channels in neurons (Plant et al., 2011; Plant et al., 2012; Qi et al., 2014; Plant et al., 2016; Welch et al., 2019).

We observe that the effects of SUMO1 differs in different parts of the neuron due to the heterogeneous subcellular distribution of sodium channel subtypes and their differential susceptibility to SUMOylation. In pyramidal neurons, the SUMO1 sensitive sodium channels, $Na_v1.2$, are in the area associated with backpropagation, i.e. in the soma, dendrites, and proximal parts of the AIS (Lorincz and Nusser, 2008; Hu et al., 2009;

Grubb et al., 2011; Plant et al., 2016). The SUMO1 insensitive $Na_v1.6$ channels, however, are located mostly in the distal part of the AIS and in the nodes of Ranvier, i.e. in the compartments associated with spike forward propagation (Caldwell et al., 2000; Lorincz and Nusser, 2008; Hu et al., 2009; Li et al., 2014; Tian et al., 2014; Plant et al., 2016). In the physiological context, this means that SUMO influences the processes mediated by $Na_v1.2$ but not $Na_v1.6$, which are spatially distributed along the neuron. The differential effect of SUMO1 on propagation speed **(Figure 6)**, in addition to the differential effect of SUMO1 on the activation curve of the I_{NaP} (**Figure 3**) supports this hypothesis.

In cortical pyramidal neurons, spike forward propagation is mediated by $Na_v1.6$, and backpropagation is mediated by $Na_v1.2$, due to the subcellular compartmentalization of these channel subtypes (Hu et al., 2009). Our evidence that SUMO1 affects the backpropagation, but not forward propagation indicates that activation of SUMOylation pathways does not affect the ongoing processing by the cortical neuronal circuits. However, SUMO1, in its physiological context, may play an important role in the regulation of spike-time-dependent plasticity of dendritic spines. The backpropagating APs invading the dendrites remove Mg^{2+} from NMDA receptor channels and trigger the long-lasting changes in synaptic strength (Markram et al., 1997; Sjöström et al., 2001; Holtmaat and Svoboda, 2009). The activation of $5\text{-}HT_{1A}$ receptors decreases the success rate of AP backpropagation and enhances the segregation of axonal and dendritic activities (Yin et al., 2017).

Unlike phosphorylation, SUMOylation of the target proteins is reported to depend on SUMO concentration (for review see (Flotho and Melchior, 2013)). SUMO acts as a

limiting factor for conjugation because of the abundance of enzymes responsible for SUMO attachment in the cytosol. Similarly, the concentration of SUMO-specific proteases that cleave the isopeptide bonds is a limiting factor for deSUMOylation. Thus, intracellular administration of the exogenous SUMO1 and SENP1 is capable of either saturating or emptying the SUMO-conjugation sites on the ion channels, respectively, reflecting the local concentrations of the peptides. However, because of the complex morphological structure of L5 pyramidal neurons, diffusion of SUMO1 and SENP1 from the somatic whole-cell pipette into the cytosol is expected to be extremely slow, with half diffusion times of several hours (Fleidervish et al., 2008). Therefore, a limitation of this study is that the concentration of these peptides is expected to be significantly lower throughout the neurons than the pipette concentration making it difficult to predict whether SUMOylation of the Na^+ and K^+ channels has reached steady state even after our 30 min protocols.

Our results demonstrate that SUMOylation of $Na_v1.2$ channels significantly increases the speed of AP backpropagation. The subsequent events and consequences due to the acceleration may need to be further investigated, for example, the change of the Ca^{2+} transient to synaptic contacts on dendrites, the alteration of local dendritic membrane excitability, and the potential effects on other neuromodulator receptors. SUMOylation might alter the time delay between the pre- and post-synaptic action potentials thereby influencing the resulting change in synaptic efficiency. Together with the synergistic effect on the excitability in cortical pyramidal neurons, our findings suggest that $Na_V1.2$ and the SUMO pathway might be a new mechanism for the regulation of action potential and neuronal function in brain.

Acknowledgments

This research was supported by The Israel Science Foundation (grant No. 1384/19) and National Institutes of Health grant R01HL10549 (to S.A.N.G.)

Author contributions

O.K. and Y.K. performed experiments. H.D., L.D.P., and S.A.N.G, created the transgenic mouse; O.K., Y.K., A.S. and I.A.F. analyzed data; S.A.N.G. and I.A.F. designed the research. O.K., Y.K., H.D., L.D.P., S.A.N.G., and I.A.F. wrote the paper.

Declaration of interests

The authors report no competing financial interests.

Star methods

KEY RESOURCES TABLE

REAGENT or RESOURCE	SOURCE	IDENTIFIER
Chemicals, Peptides, and Recombinant Proteins		
Human SUMO1	RND Systems	UL-740

Human SENP1	RND Systems	E-700
Experimental Models: Organisms/Strains		
Mouse: C57BL/6N-Scn2a-K38Q$^{Mut/+}$	Biocytogen	EGE-ZY-016
Software and Algorithms		
NEURON 8.1	Yale university	SCR_005393

LEAD CONTACT AND MATERIALS AVAILABILITY

Further Information and requests for resources and reagents should be directed to the Lead Contacts. Materials generated through this work are available from the Lead Contact upon reasonable request.

EXPERIMENTAL MODEL

Animals

The C57BL/6N-Na$_v$1.2-K38Q$^{Mut/+}$ mice were generated by and obtained from Biocytogen (Wakefield, Massachusetts). The Na$_v$1.2-K38Q$^{Mut/+}$ mice backcrossed against C57BL/6N for 5 generations. Both male and female mice were used without bias. This study was carried out at the Ben-Gurion University of the Negev in accordance with the recommendations of guidelines for the welfare of experimental animals. Animal experiments were approved by the Institutional Animal Care and Use Committee of Ben-Gurion University.

METHOD DETAILS

Generation of the Scn2a-K38Q knock in mice model

The Scn2a-K38Q mutation knock in mice were generated using a CRISPR/Cas9 based approach. Briefly, two sgRNAs were designed using the CRISPR design tool (http://www.sanger.ac.uk/) to target the region of the exon 1 of the Scn2a gene locus, then screened for on-target activity using a Universal CRISPR Activity Assay (UCATM, Biocytogen Pharmaceuticals Co., Ltd). The T7 promoter sequence was added to the Cas9 or sgRNA template by PCR amplification *in vitro*. Different concentrations of the donor vector and the purified, *in vitro*-transcribed Cas9 mRNA and sgRNA were mixed and co-injected into the cytoplasm of one-cell stage fertilized egg from a C57BL/6N mouse. The injected zygotes were transferred into the oviducts of Kunming pesudopregnant females to generate F0 mice. PCR and sequencing verified founder pups harboring the intended mutation were then crossed with wild-type mice for germline transmission. The germline sequence was confirmed by PCR, sequencing and Southern blot analysis.

Slice preparation and whole-cell recording

Experiments were performed on L5 pyramidal neurons in 300 µm thick mouse cortical sagittal slices using previously described techniques (Fleidervish et al., 2010; Katz et al., 2018). The P18-P24 mice of either sex (Envigo, Israel) were anesthetized with Isoflurane, decapitated, and the brains were placed in cold (4-8°C) oxygenated (95% O_2–5% CO_2) artificial cerebrospinal fluid (aCSF). The composition of the aCSF was (in mM): 124 NaCl, 3 KCl, 2 $CaCl_2$, 2 $MgSO_4$, 1.25 NaH_2PO_4, 26 $NaHCO_3$, and 10 glucose (all

chemicals obtained from Sigma Aldrich); pH was 7.4 when bubbled with 95% O_2/CO_2. Slices were cut on a vibratome (VT1200, Leica) and placed in a holding chamber containing oxygenated aCSF at room temperature; they were transferred to a recording chamber after at least 30 mins of incubation.

The cells were viewed with a 40 or 60 × water-immersion lens in a BX51WI microscope (Olympus) mounted on an X–Y translation stage (Luigs and Neumann, Germany). Somatic whole-cell recordings were made using patch pipettes pulled from thick-walled borosilicate glass capillaries (1.5-mm outer diameter; Science Products, Germany). The pipette solution for whole-cell voltage-clamp experiments contained (in mM): 135 CsCl, 2 $MgCl_2$, 4 NaCl, 10 HEPES, pH adjusted to 7.3 with CsOH (all chemicals obtained from Sigma Aldrich) and it was supplemented with 2 mM of Na^+ -sensitive dye, SBFI tetra-ammonium salt (ThermoFisher Scientific) (Minta and Tsien, 1989). When filled with this solution, pipettes had resistance of 3–6 MΩ. Voltage-clamp recordings from L5 neurons visually identified using IR-DIC optics (Stuart et al., 1993) were made with a MultiClamp 700B amplifier equipped with CV-7B headstage (Molecular Devices). Data were low-pass–filtered at 2 kHz (−3 dB, 4-pole Bessel filter) and digitized at 10 kHz using Digidata 1322A digitizer driven by PClamp 9 software (Molecular Devices). Care was taken to maintain the access resistance as low as possible (usually 6–7 MΩ and always less than 10 MΩ); series resistance was 80% compensated using the built-in circuitry of the amplifier. Ca^{2+} currents were blocked by adding 200 µM Cd^{2+} to the bath. Voltages were not corrected for liquid junction potential. The recordings were made at room temperature (20 ± 1 °C). Current-clamp recordings were made with a MultiClamp 700B amplifier (Molecular Devices). Data were low-pass–filtered at 30 kHz (−3 dB,

four-pole Bessel filter) and digitized at 100 kHz. Somatic recordings were made by using patch pipettes pulled from thick-walled borosilicate glass capillaries (1.5 mm outer diameter; Hilgenberg). Pipettes had resistances of 5-7 MΩ when filled with K gluconate based solution with the following composition (in mM): 130 K–gluconate, 6 KCl, 2 $MgCl_2$, 4 NaCl, and 10 Hepes, with pH adjusted to 7.25 with KOH. Solution was supplemented with 2 mM of sodium-binding benzofuran isophthalate (SBFI, Molecular Probes).

EPSP were elicited by delivering brief (0.1 ms) current pulses using optically coupled ISO-Flex Stimulus Isolator (AMPI, Jerusalem) via the bipolar Tungsten electrode (WPI, 0.01 MΩ) placed in the vicinity of the postsynaptic neuron. The stimulation intensity was carefully controlled to elicit monosynaptic, subthreshold EPSPs with a latency of <1 ms post-stimulus.

SUMO (1 nM) and SENP (0.25 nM) were delivered to the neurons intracellularly via the whole cell recording pipette.

Measuring propagation speed

To measure action potential propagation velocity, we performed simultaneous recordings from soma and axon of L5 pyramidal neurons. The whole-cell current clamp somatic recordings were obtained, and the neurons were filled for 15 min with Na^+ indicator, SBFI (2 mM), as described above. Trains of five action potentials were elicited by delivering brief current steps via the somatic pipette, and axons were identified by their characteristic Na^+ signals. Another pipette filled with the extracellular solution supplemented with SBFI (2 mM), with a resistance of 15–20 MΩ, was positioned at

different points along the axon in a loose-patch configuration. At each point along the axon, 100 single APs were elicited by delivering brief current pulses via the somatic electrode, and axonal action currents were simultaneously recorded. Both pipettes were coated to within ~100 μm of the tip with Parafilm (Sigma-Aldrich) to minimize stray capacitance. Currents were low-pass–filtered at 100 kHz (−3 dB, four-pole Bessel filter) and digitized at 200 kHz. To identify the time delays between the somatic and the axonal signals, they were aligned to the times of maximal rate-of-rise of the somatic APs and averaged. Then, the differences between the times of peak of the axonal action currents and times of maximal rate-of-rise of the somatic APs were calculated.

Sodium imaging

Imaging experiments were performed as described previously (Baranauskas et al., 2013; Shvartsman et al., 2021). SBFI fluorescence was excited by using a high-intensity LED device [385 ± 4 nm; Prizmatix], and the emission was collected by using a modified Olympus U-MNU2 filter set (400-nm dichroic mirror; 420-nm long pass emission filter). The fluorescent response of SBFI was recorded using a back-illuminated 80 × 80 pixel cooled camera (NeuroCCDSMQ; RedShirt Imaging) at 500 frames/second acquisition speed controlled by Neuroplex software. Indicator bleaching was corrected by subtracting an equivalent blank trace without electrical stimulation.

Data analysis

Data analysis was accomplished using pCLAMP10 software (Molecular Devices) and Origin 6.0 (OriginLab). If not otherwise noted, values are given as mean ± S.E. Student's *t* test was used for statistical analysis.

Modeling

Numerical simulations were performed in the NEURON simulation environment (Hines and Carnevale, 1997). Unless otherwise stated, electrophysiological parameters and dynamic $[Na^+]_i$ changes were studied in a simplified compartmental model that encompassed the fundamental morphological and electrical features of layer 5 pyramidal neurons as described previously (Baranauskas et al., 2013; Shvartsman et al., 2021).

In the model, the 1.2 µm-thick AIS extended over the first 40 - 50 µm of the axon. The subsequent segment (length, 50 µm; diameter, 1.2 µm) was myelinated. The nodes were 1 µm long and had a diameter of 1.2 µm, and the myelinated internodes were 2 µm long and had a diameter of 1.2 µm. In addition to the axon, the soma (length 35 μm, diameter: 23 μm) gave rise to the apical dendrite (length 350 μm, diameter 3.5 μm) and two basal dendrites (length 200 μm, diameter 1.2 μm). For spatial precision, all compartments were divided into 1 µm long isopotential segments.

The passive electrical properties R_m, C_m, and R_i were set to 25,000 Ω cm^2, 1 µF cm^{-2}, and 150 Ω cm, respectively, uniformly. The myelinated internode had C_m of 0.5 µF·cm^{-2}. The resting membrane potential at the soma was set to −75 mV.

All simulations were run with 1-µs time steps, and the nominal temperature was set to 18 °C. The model used a Hodgkin-Huxley–based Na^+ conductance. The steady state activation and inactivation characteristics of the $Na_v1.6$ channels were left-shifted by 6 mV and 3 mV, respectively, compared with the $Na_v1.2$ channels. The Na^+ conductance was set to 200 pS µm^{-2} in the soma, 200 pS µm^{-2} in the apical dendrite, 40 pS µm^{-2} in the basal dendrites, 1,200 pS µm^{-2} in the nodes of Ranvier; no Na^+ channels

514 were present in the internodes. The model included Kv and Kv1 K^+ channels with
515 kinetics and density as previously described. The K^+ equilibrium potential was set to −85
516 mV.

517 The AIS contained variable Na^+ channel density as described by Baranauskas et al.
518 (Baranauskas et al., 2013). At both proximal and medial parts of the AIS the gNa was
519 represented only by $Na_v1.2$ channels. The gNa at the proximal AIS segment incremented
520 linearly from 200 pS μm^{-2} to 800 pS μm^{-2}, the middle AIS part had a constant gNa of 800
521 pS μm^{-2}. The distal AIS part was populated by $Na_v1.6$ channels with density
522 decrementing from 800 to 0 pS μm^{-2}.

523 Diffusion of Na^+ ions was modeled as the exchange of Na^+ ions between adjacent
524 neuronal compartments using the intrinsic protocols in NEURON, assuming a diffusion
525 coefficient of 0.6 μm^2 ms^{-1} (Kushmerick and Podolsky, 1969; Fleidervish et al., 2010).
526 The resting intracellular and the extracellular Na^+ concentrations were set to 4 and 151
527 mmol/L, respectively.

528

529

530 # Figures and Legends

531

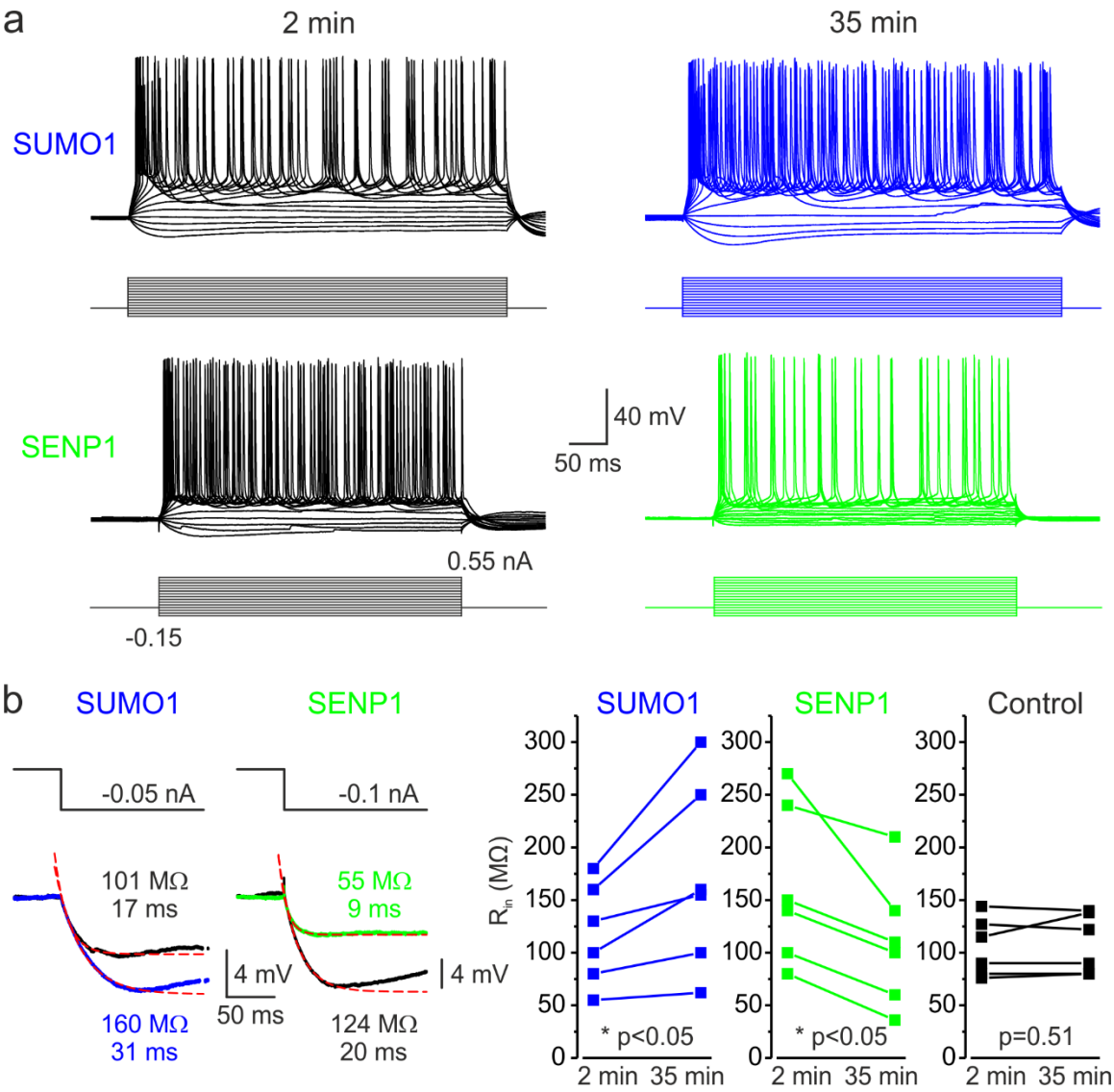

532

533 **Figure 1. SUMOylation and deSUMOylation have opposing effects on the**

534 **excitability of Layer 5 pyramidal neurons.**

535 **(a)** Current clamp, whole-cell recordings from L5 neurons 2 mins after the break-in to

536 whole-cell mode (black) and 35 mins later demonstrate time-dependent effects of

SUMO1 (blue) or SENP1 (green) dialysis on firing frequency. Voltage responses were elicited by injecting 400 ms long current pulses which started at -0.15 nA and incremented by 50 pA.

(b) SUMO1 and SENP1 have opposite effects on passive membrane properties. *Left*, voltage responses to a small hyperpolarizing current pulse injection immediately after the break-in (black) and following SUMO1 (blue) or SENP1 (green) dialysis via the whole-cell pipette. Red dashed lines are the best exponential fits of the voltage responses. Notice that the amplitude of voltage deflection and the membrane time constant were enhanced by SUMO1 and decreased by SENP1 dialysis. *Right*, apparent input resistance (R_{in}) increased in SUMO1 dialyzed neurons, whereas it decreased in SENP1 dialyzed cells. The lines connect the paired R_{in} values obtained from the same individual neuron at 2 min and 35 min of recording with SUMO1 (blue), SENP1 (green), and control solution filled pipette (black).

Figure 1 - Figure Supplement 1. The effects of SUMO1 and SENP1 on input/output gain.

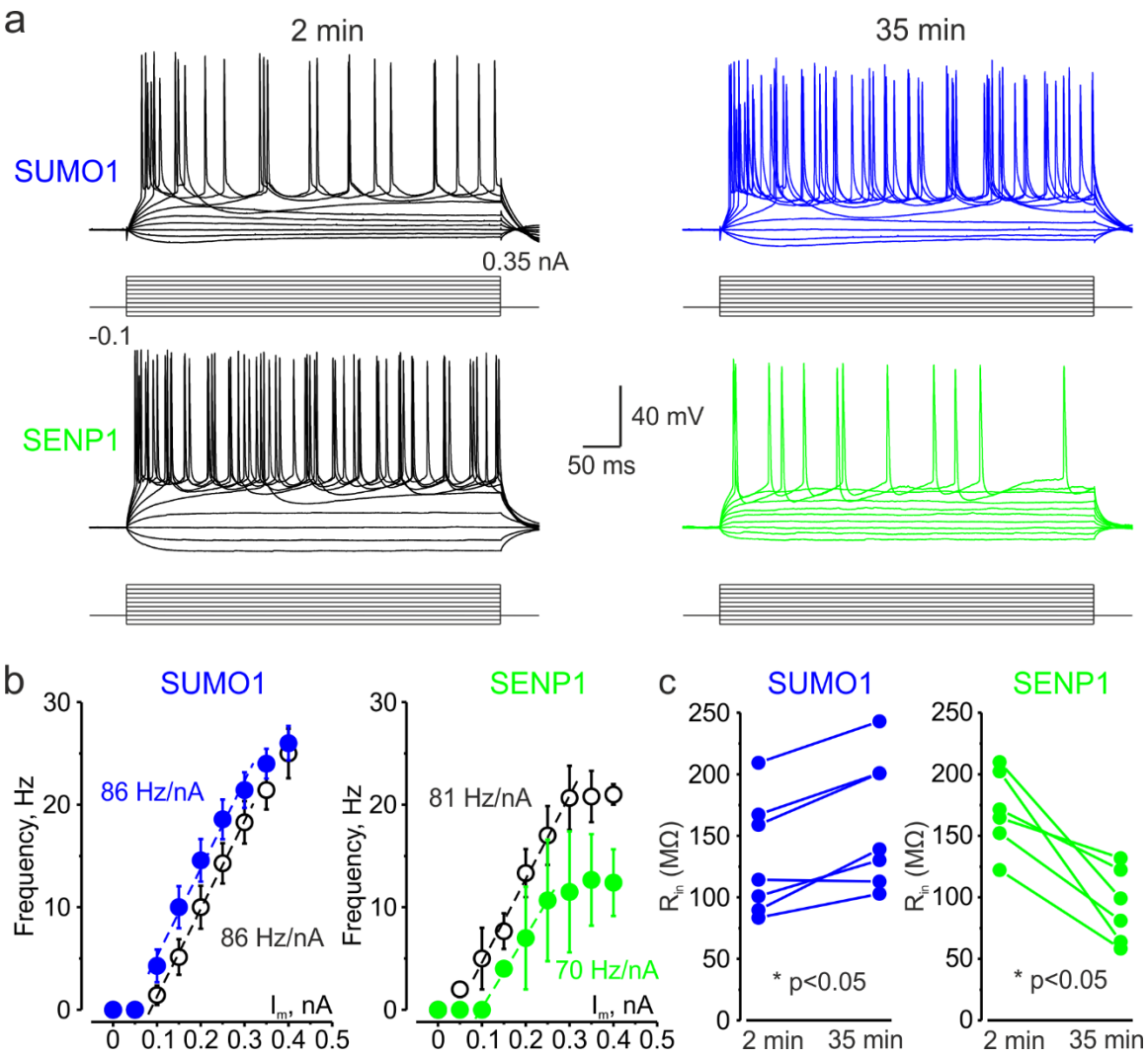

Figure 2. In L5 $Na_v1.2$-Lys38Gln mutant neurons, SUMO1 and SENP1 do not affect the gain of the input-output curve.

(a) Current clamp, whole-cell recordings from L5 $Na_v1.2$-Lys38Gln mutant neurons immediately after the break-in (black) and following SUMO1 (blue) or SENP1 (green) dialysis. Voltage responses were elicited by injecting 400 ms long current pulses which started at -0.15 nA and incremented by 50 pA.

(b) The F-I characteristic of $Na_v1.2$-Lys38Gln mutant neurons obtained immediately after the break-in (black) and following SUMO1 (n=6, blue) or SENP1 (n=8, green) dialysis via the whole-cell pipette. Notice the opposite effects of SUMO1 and SENP1 on the position of the F-I curve over the current axis. Both treatments had little to no effect on the slope of the F-I curve.

(c) The R_{in} increased over time in SUMO1 dialyzed $Na_v1.2$-Lys38Gln mutant neurons, whereas it decreased in SENP1 dialyzed cells. Dots represent the values for the R_{in} measured in individual SUMO1 (blue), SENP1 (green) immediately after the break-in and following SUMO1 or SENP1 dialysis.

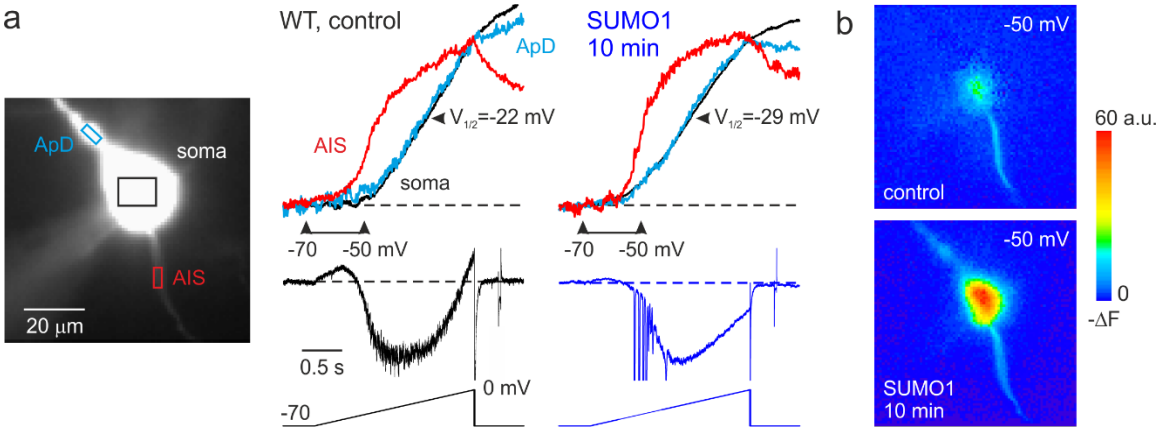

Figure 3. SUMO1 causes a leftward shift of activation kinetics of I_{NaP} in pyramidal cells from wild type but not from $Na_v1.2$-Lys38Gln mutant mice.

(a) *Left*, WT L5 pyramidal neuron filled with SBFI-containing, Cs^+-based solution via a somatic patch pipette, as seen during the fluorescence imaging experiment with a NeuroCCD-SMQ camera. *Right*, I_{NaP} and normalized somatic (black), axonal (red), and dendritic (cyan) ΔF transients elicited by 2 s long voltage ramp from -70 mV to 0 mV immediately after the break-in and following 10 minutes of dialysis with SUMO1. Notice the leftward shift in I_{NaP} activation in soma, dendrite, and to a lesser extent, in AIS.

(b) Pseudocolor maps of the ramp elicited ΔF changes between the times marked by the arrowheads in A. *Top*, voltage ramp from −70 to −50 mV elicited Na^+ elevation mostly in the AIS. *Bottom*, following the SUMO1 dialysis, voltage ramp from −70 to -50 mV elicited large Na^+ signals also in the soma and dendrites.

Figure 3 - Figure Supplement 1. $V_{1/2}$ of I_{NaP} activation in the soma (black) and AIS (red) of WT pyramidal neurons immediately after the break-in and following 10 minutes of dialysis with SUMO1.

Figure 3 - Figure Supplement 2. $V_{1/2}$ of I_{NaP} activation in the soma (black) and AIS (red) of pyramidal neurons of animals carrying $Na_v1.2$-Lys38Gln mutation, immediately after the break-in, and following 10 minutes of dialysis with SUMO1.

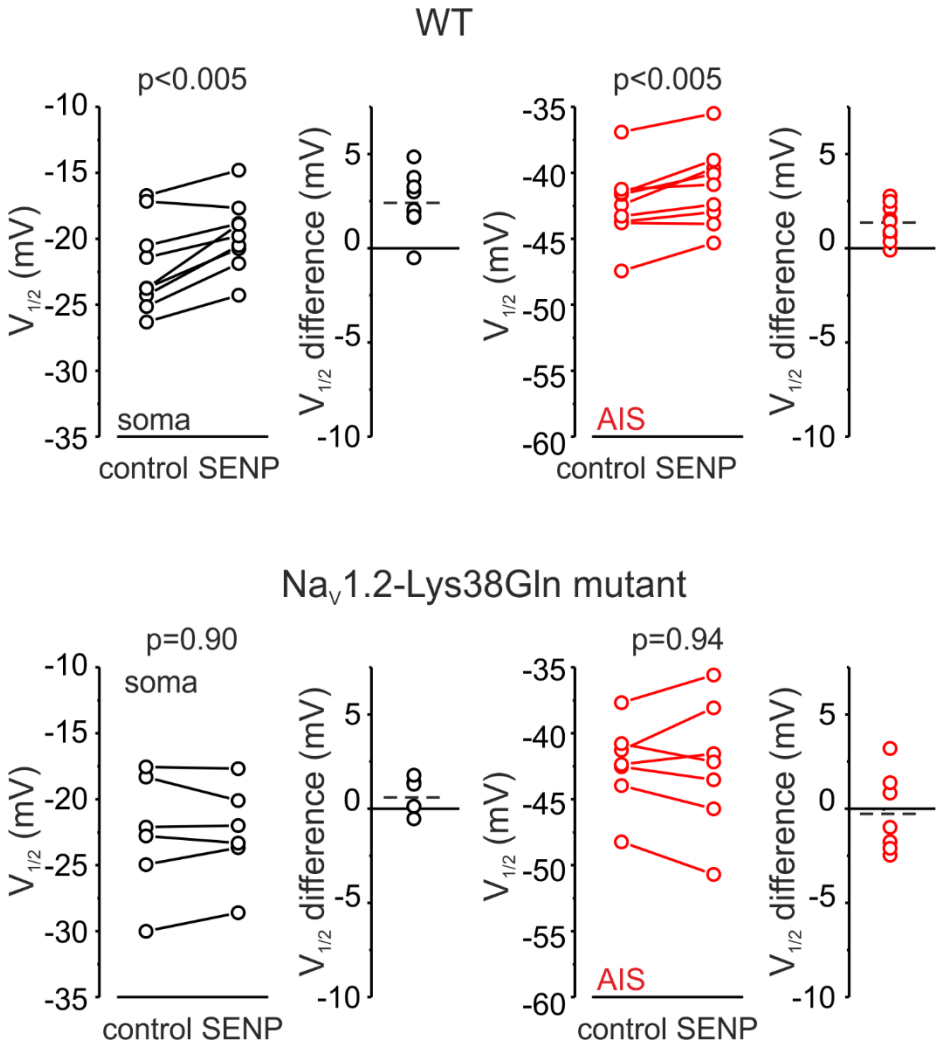

599

600

601 **Figure 4.** SENP1 causes a rightward shift of activation kinetics of I_{NaP} in pyramidal cells

602 from wild type but not from $Na_v1.2$-Lys38Gln mutant mice.

603 $V_{1/2}$ of I_{NaP} activation in the soma (black) and AIS (red) of WT (top) and Nav1.2-

604 Lys38Gln mutant (bottom) pyramidal neurons immediately after the break-in and

605 following 10 minutes of dialysis with SENP1. Dots represent the results of $V_{1/2}$

606 measurements in individual cells.

607

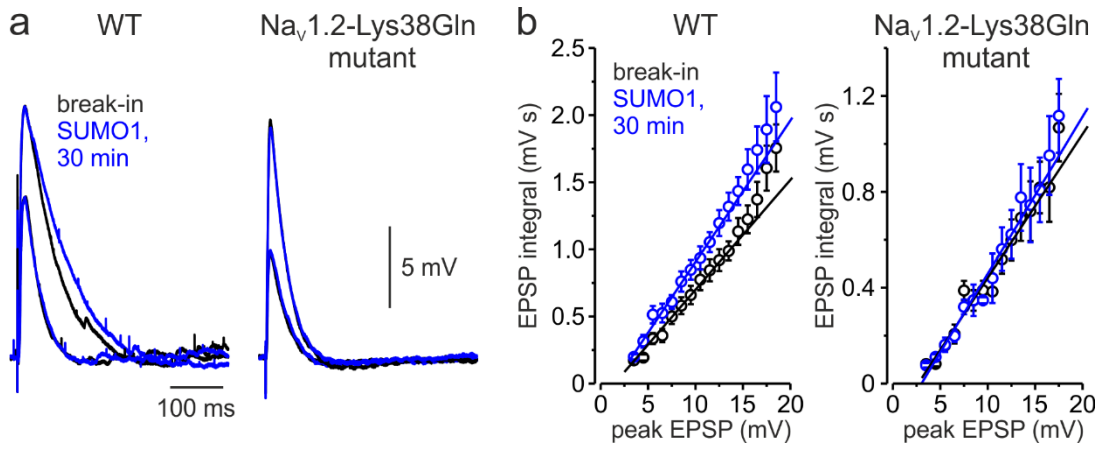

Figure 5. Effect of SUMO1 on voltage-dependent amplification of EPSPs in pyramidal neurons from wild type and $Na_v1.2$-Lys38Gln mutant mice.

(a) Comparison of small and large EPSPs evoked in WT and $Na_v1.2$-Lys38Gln mutant pyramidal neurons immediately after the brake-in (black) and following the SUMO1 dialysis (blue). Notice the slower decay time constant of larger EPSP following SUMO1 dialysis in WT neuron.

(b) The mean EPSP integral as a function of peak EPSP amplitude after the brake-in (black) and following the SUMO1 dialysis (blue) of the WT (n=6) and $Na_v1.2$-Lys38Gln mutant (n=6) pyramidal neurons. Notice amplification of smaller EPSPs in SUMO1 dialyzed WT cells.

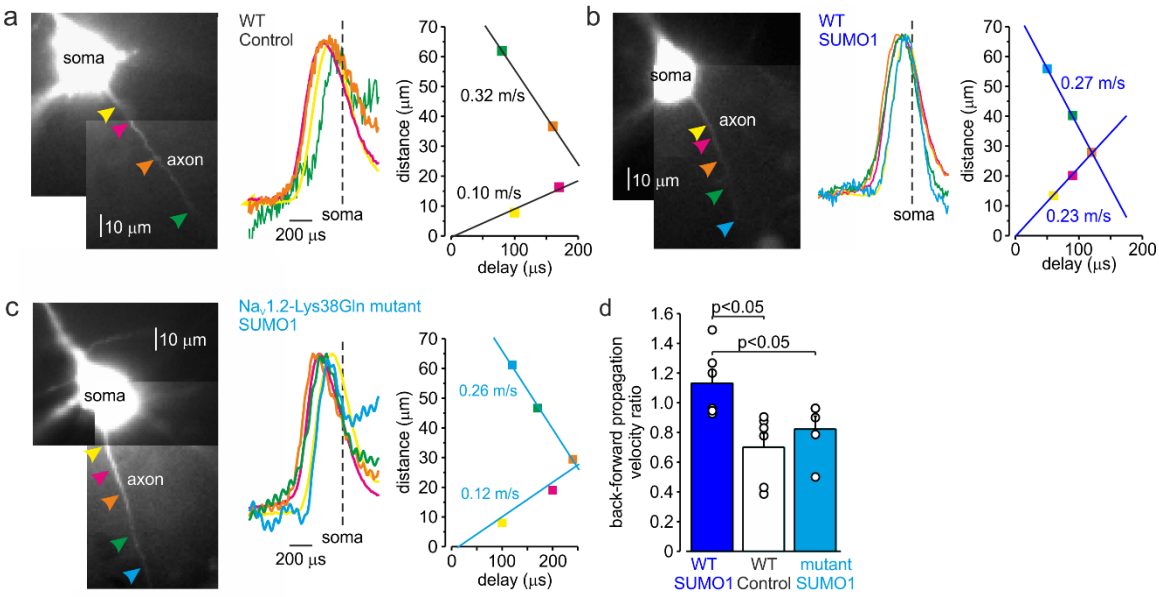

Figure 6. SUMOylation differentially affects the velocity of forward- and back-propagating action potentials.

(a) *Left*, normalized averaged action currents (n = 500) elicited by a single AP at the axonal regions indicated by arrows, to demonstrate the difference in the delay of their onset. The dashed vertical line corresponds to the time of dB/dt_{max} of the somatic action potential. *Right*, distance from the edge of the soma as a function of delay of spike initiation plotted. Note that AP initiates in a region located between the pink and brown arrows and propagates with an apparent conduction velocity of ~0.32 and ~0.10 m/s forward and backward, respectively.

(b) In SUMO1 dialyzed neurons, there was little difference in apparent conduction velocity of forward- and back-propagating action potential (~0.27 vs 0.23 m/s, respectively).

637 **(c)** In a representative neuron from $Na_v1.2$-Lys38Gln mutant animal, SUMO1 dialysis
638 does not change the velocity of backpropagating action potential (~0.26 vs 0.12 m/s for
639 forward and backpropagation, respectively).

640 **(d)** SUMOylation causes a significant increase in the back/forward propagation velocity
641 ratio. Each dot represents the velocity measurement in individual control (n=6, black),
642 SUMO1 dialyzed WT (n=6, blue) and SUMO1 dialyzed $Na_v1.2$-Lys38Gln mutant (n=4,
643 blue) axon.

644

645 **Figure 6 - Figure Supplement 1.** In computational models, SUMOylation of $Na_v1.2$
646 channels selectively accelerates spike backpropagation.

647 **(e)** In computational models, SUMOylation of $Na_v1.2$ channels selectively accelerates
648 spike backpropagation. *Left*, Schematic drawing of L5 pyramidal neuron with $Na_v1.2$
649 (red) present in the soma and proximal AIS and $Na_v1.6$ (green) localized in the distal AIS
650 and nodes of Ranvier. *Right*, the delays of AP initiation plotted against distance from the
651 edge of the soma in the model of a neuron under control conditions (black) and following
652 the SUMO1 dialysis. Straight lines are linear fits of the linear portions of the delay-
653 distance relationship with their slopes representing the velocities of back- and forward-
654 propagation velocities. Note that SUMOylation of $Na_v1.2$ channels selectively enhances
655 the velocity of backpropagating AP.

656

References

Astman N, Gutnick MJ, Fleidervish IA (2006) Persistent sodium current in layer 5 neocortical neurons is primarily generated in the proximal axon. J Neurosci 26:3465-3473.

Baranauskas G, David Y, Fleidervish IA (2013) Spatial mismatch between the Na+ flux and spike initiation in axon initial segment. Proc Natl Acad Sci U S A 110:4051-4056.

Bean BP (2007) The action potential in mammalian central neurons. Nat Rev Neurosci 8:451-465.

Bender KJ, Uebele VN, Renger JJ, Trussell LO (2012) Control of firing patterns through modulation of axon initial segment T-type calcium channels. J Physiol 590:109-118.

Caldwell JH, Schaller KL, Lasher RS, Peles E, Levinson SR (2000) Sodium channel Na(v)1.6 is localized at nodes of ranvier, dendrites, and synapses. Proc Natl Acad Sci U S A 97:5616-5620.

Cantrell AR, Catterall WA (2001) Neuromodulation of Na+ channels: an unexpected form of cellular plasticity. Nat Rev Neurosci 2:397-407.

Cantrell AR, Ma JY, Scheuer T, Catterall WA (1996) Muscarinic modulation of sodium current by activation of protein kinase C in rat hippocampal neurons. Neuron 16:1019-1026.

Chance FS, Abbott LF, Reyes AD (2002) Gain modulation from background synaptic input. Neuron 35:773-782.

Chen Y, Yu FH, Sharp EM, Beacham D, Scheuer T, Catterall WA (2008) Functional properties and differential neuromodulation of Na(v)1.6 channels. Mol Cell Neurosci 38:607-615.

Deisz RA, Fortin G, Zieglgänsberger W (1991) Voltage dependence of excitatory postsynaptic potentials of rat neocortical neurons. J Neurophysiol 65:371-382.

Fleidervish IA, Libman L, Katz E, Gutnick MJ (2008) Endogenous polyamines regulate cortical neuronal excitability by blocking voltage-gated Na+ channels. Proc Natl Acad Sci U S A 105:18994-18999.

Fleidervish IA, Lasser-Ross N, Gutnick MJ, Ross WN (2010) Na+ imaging reveals little difference in action potential-evoked Na+ influx between axon and soma. Nat Neurosci 13:852-860.

Flotho A, Melchior F (2013) Sumoylation: a regulatory protein modification in health and disease. Annu Rev Biochem 82:357-385.

Goldin AL, Barchi RL, Caldwell JH, Hofmann F, Howe JR, Hunter JC, Kallen RG, Mandel G, Meisler MH, Netter YB, Noda M, Tamkun MM, Waxman SG, Wood JN, Catterall WA (2000) Nomenclature of voltage-gated sodium channels. Neuron 28:365-368.

Grubb MS, Shu Y, Kuba H, Rasband MN, Wimmer VC, Bender KJ (2011) Short- and long-term plasticity at the axon initial segment. J Neurosci 31:16049-16055.

698 Hines ML, Carnevale NT (1997) The NEURON simulation environment. Neural Comput
699 9:1179-1209.
700 Holtmaat A, Svoboda K (2009) Experience-dependent structural synaptic plasticity in the
701 mammalian brain. Nat Rev Neurosci 10:647-658.
702 Hu W, Tian C, Li T, Yang M, Hou H, Shu Y (2009) Distinct contributions of Na(v)1.6
703 and Na(v)1.2 in action potential initiation and backpropagation. Nat Neurosci
704 12:996-1002.
705 Katz E, Stoler O, Scheller A, Khrapunsky Y, Goebbels S, Kirchhoff F, Gutnick MJ, Wolf
706 F, Fleidervish IA (2018) Role of sodium channel subtype in action potential
707 generation by neocortical pyramidal neurons. Proc Natl Acad Sci U S A
708 115:E7184-E7192.
709 Kole MH, Stuart GJ (2012) Signal processing in the axon initial segment. Neuron
710 73:235-247.
711 Kushmerick MJ, Podolsky RJ (1969) Ionic mobility in muscle cells. Science 166:1297-
712 1298.
713 Lezmy J, Lipinsky M, Khrapunsky Y, Patrich E, Shalom L, Peretz A, Fleidervish IA,
714 Atali B (2017) M-current inhibition rapidly induces a unique CK2-dependent
715 plasticity of the axon initial segment. Proc Natl Acad Sci U S A 114:E10234-
716 E10243.
717 Li T, Tian C, Scalmani P, Frassoni C, Mantegazza M, Wang Y, Yang M, Wu S, Shu Y
718 (2014) Action potential initiation in neocortical inhibitory interneurons. PLoS
719 Biol 12:e1001944.
720 Lorincz A, Nusser Z (2008) Cell-type-dependent molecular composition of the axon
721 initial segment. J Neurosci 28:14329-14340.
722 Lorincz A, Nusser Z (2010) Molecular identity of dendritic voltage-gated sodium
723 channels. Science 328:906-909.
724 Markram H, Lubke J, Frotscher M, Sakmann B (1997) Regulation of synaptic efficacy by
725 coincidence of postsynaptic APs and EPSPs. Science 275:213-215.
726 Maurice N, Tkatch T, Meisler M, Sprunger LK, Surmeier DJ (2001) D1/D5 dopamine
727 receptor activation differentially modulates rapidly inactivating and persistent
728 sodium currents in prefrontal cortex pyramidal neurons. J Neurosci 21:2268-2277.
729 Minta A, Tsien RY (1989) Fluorescent indicators for cytosolic sodium. J Biol Chem
730 264:19449-19457.
731 Plant LD, Marks JD, Goldstein SA (2016) SUMOylation of NaV1.2 channels mediates
732 the early response to acute hypoxia in central neurons. Elife 5.
733 Plant LD, Dowdell EJ, Dementieva IS, Marks JD, Goldstein SA (2011) SUMO
734 modification of cell surface Kv2.1 potassium channels regulates the activity of rat
735 hippocampal neurons. J Gen Physiol 137:441-454.
736 Plant LD, Zuniga L, Araki D, Marks JD, Goldstein SA (2012) SUMOylation silences
737 heterodimeric TASK potassium channels containing K2P1 subunits in cerebellar
738 granule neurons. Sci Signal 5:ra84.

739 Plant LD, Xiong D, Romero J, Dai H, Goldstein SAN (2020) Hypoxia Produces Pro-
740 arrhythmic Late Sodium Current in Cardiac Myocytes by SUMOylation of
741 Na(V)1.5 Channels. Cell Rep 30:2225-2236.e2224.
742 Plant LD, Dementieva IS, Kollewe A, Olikara S, Marks JD, Goldstein SA (2010) One
743 SUMO is sufficient to silence the dimeric potassium channel K2P1. Proc Natl
744 Acad Sci U S A 107:10743-10748.
745 Qi Y, Wang J, Bomben VC, Li DP, Chen SR, Sun H, Xi Y, Reed JG, Cheng J, Pan HL,
746 Noebels JL, Yeh ET (2014) Hyper-SUMOylation of the Kv7 potassium channel
747 diminishes the M-current leading to seizures and sudden death. Neuron 83:1159-
748 1171.
749 Rajan S, Plant LD, Rabin ML, Butler MH, Goldstein SA (2005) Sumoylation silences the
750 plasma membrane leak K+ channel K2P1. Cell 121:37-47.
751 Rasband MN (2010) The axon initial segment and the maintenance of neuronal polarity.
752 Nat Rev Neurosci 11:552-562.
753 Rush AM, Dib-Hajj SD, Waxman SG (2005) Electrophysiological properties of two
754 axonal sodium channels, Nav1.2 and Nav1.6, expressed in mouse spinal sensory
755 neurones. J Physiol 564:803-815.
756 Shvartsman A, Kotler O, Stoler O, Khrapunsky Y, Melamed I, Fleidervish IA (2021)
757 Subcellular distribution of persistent sodium conductance in cortical pyramidal
758 neurons. J Neurosci 41:6190-6201.
759 Sjöström PJ, Turrigiano GG, Nelson SB (2001) Rate, timing, and cooperativity jointly
760 determine cortical synaptic plasticity. Neuron 32:1149-1164.
761 Smith MR, Smith RD, Plummer NW, Meisler MH, Goldin AL (1998) Functional analysis
762 of the mouse Scn8a sodium channel. J Neurosci 18:6093-6102.
763 Stuart G (1999) Voltage-activated sodium channels amplify inhibition in neocortical
764 pyramidal neurons. Nat Neurosci 2:144-150.
765 Stuart G, Sakmann B (1995) Amplification of EPSPs by axosomatic sodium channels in
766 neocortical pyramidal neurons. Neuron 15:1065-1076.
767 Stuart G, Spruston N, Sakmann B, Hausser M (1997) Action potential initiation and
768 backpropagation in neurons of the mammalian CNS. Trends Neurosci 20:125-131.
769 Stuart GJ, Sakmann B (1994) Active propagation of somatic action potentials into
770 neocortical pyramidal cell dendrites. Nature 367:69-72.
771 Stuart GJ, Dodt HU, Sakmann B (1993) Patch-clamp recordings from the soma and
772 dendrites of neurons in brain slices using infrared video microscopy. Pflugers
773 Arch 423:511-518.
774 Tian C, Wang K, Ke W, Guo H, Shu Y (2014) Molecular identity of axonal sodium
775 channels in human cortical pyramidal cells. Front Cell Neurosci 8:297.
776 Welch MA, Forster LA, Atlas SI, Baro DJ (2019) SUMOylating Two Distinct Sites on
777 the A-type Potassium Channel, Kv4.2, Increases Surface Expression and
778 Decreases Current Amplitude. Frontiers in molecular neuroscience 12:144.
779 Xiong D, Li T, Dai H, Arena AF, Plant LD, Goldstein SAN (2017) SUMOylation
780 determines the voltage required to activate cardiac I(Ks) channels. Proc Natl Acad
781 Sci U S A 114:E6686-e6694.

Yin L, Rasch MJ, He Q, Wu S, Dou F, Shu Y (2017) Selective Modulation of Axonal Sodium Channel Subtypes by 5-HT1A Receptor in Cortical Pyramidal Neuron. Cereb Cortex 27:509-521.

Zhou W, Goldin AL (2004) Use-dependent potentiation of the Nav1.6 sodium channel. Biophys J 87:3862-3872.

Figure Supplements

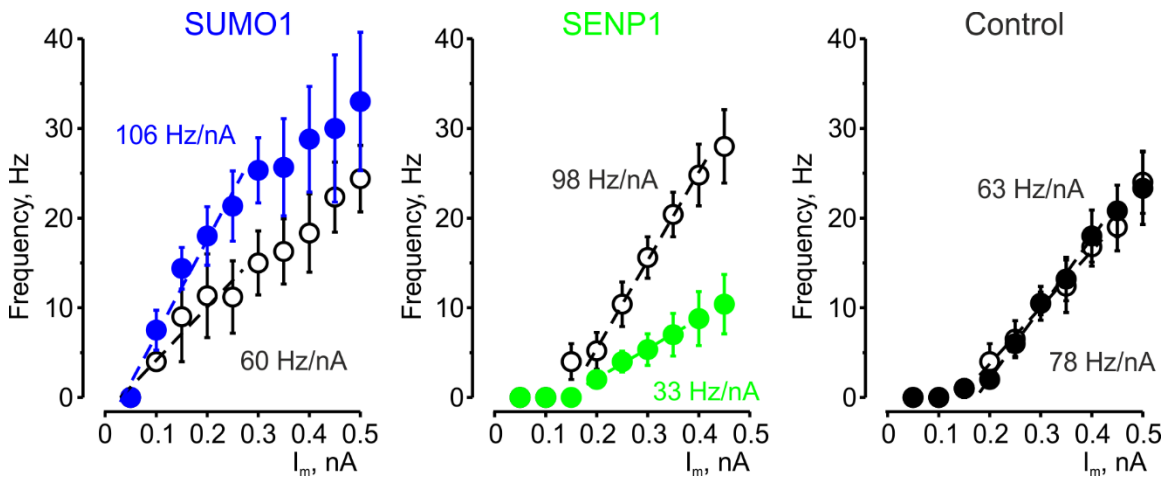

Figure 1 - Figure Supplement 1. The effects of SUMO1 and SENP1 on input/output gain.

The frequency–current (F-I) characteristic of L5 pyramidal neurons, constructed by plotting the mean instantaneous spike frequency as a function of depolarizing current pulse amplitude obtained immediately after the break-in (black) and following SUMO1 (n=6, blue) or SENP1 (n=8, green) dialysis via the whole-cell pipette. Notice that the F-I curve was shifted to the left and became steeper in SUMO1 dialyzed neurons, whereas in SENP1 dialyzed cells the F-I characteristics was displaced to the right and its slope decreased compared with control. The F-I curve showed no significant change in control recordings (n=6).

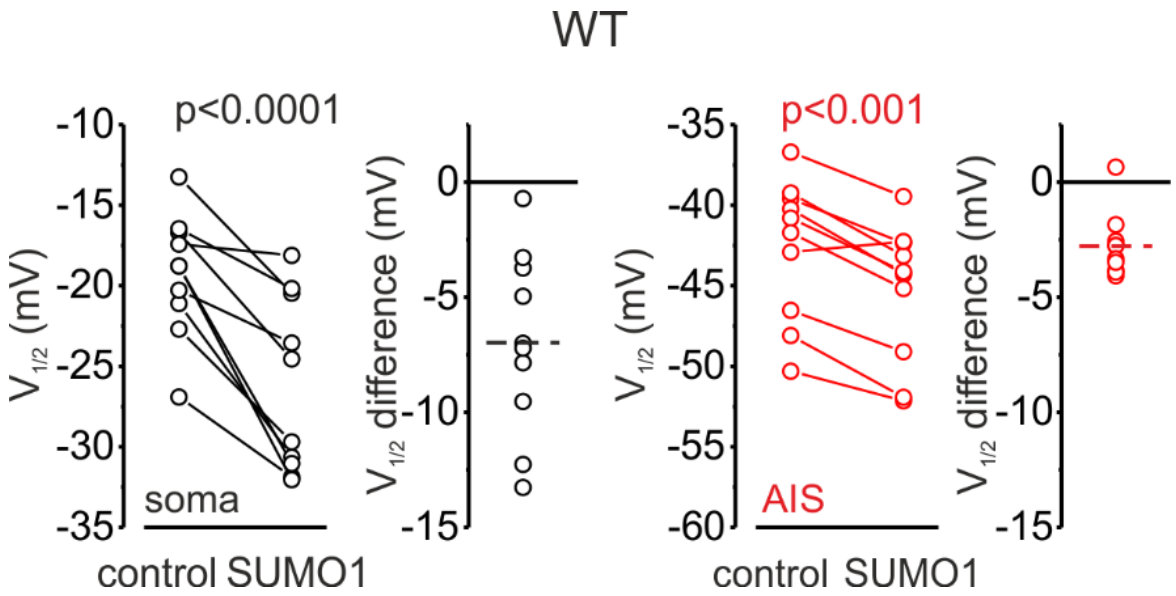

Figure 3 - Figure Supplement 1. $V_{1/2}$ of I_{NaP} activation in the soma (black) and AIS (red) of WT pyramidal neurons immediately after the break-in and following 10 minutes of dialysis with SUMO1. Dots represent the results of $V_{1/2}$ measurements in individual cells.

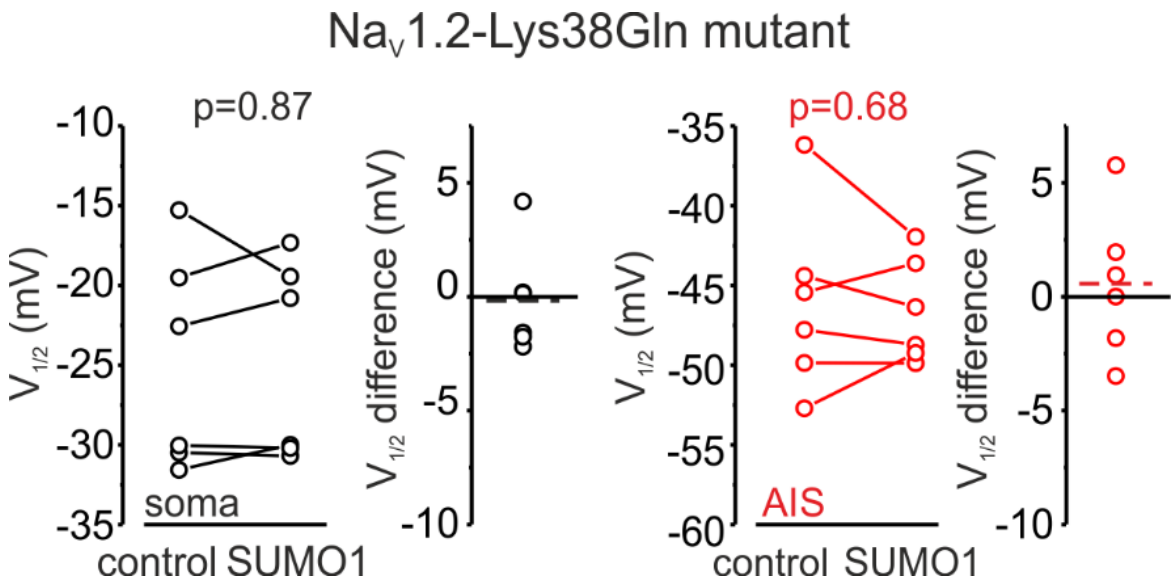

Figure 3 - Figure Supplement 2. $V_{1/2}$ of I_{NaP} activation in the soma (black) and AIS (red) of pyramidal neurons of animals carrying $Na_v1.2$-Lys38Gln mutation, immediately after the break-in, and following 10 minutes of dialysis with SUMO1. Dots represent the results of $V_{1/2}$ measurements in individual cells.

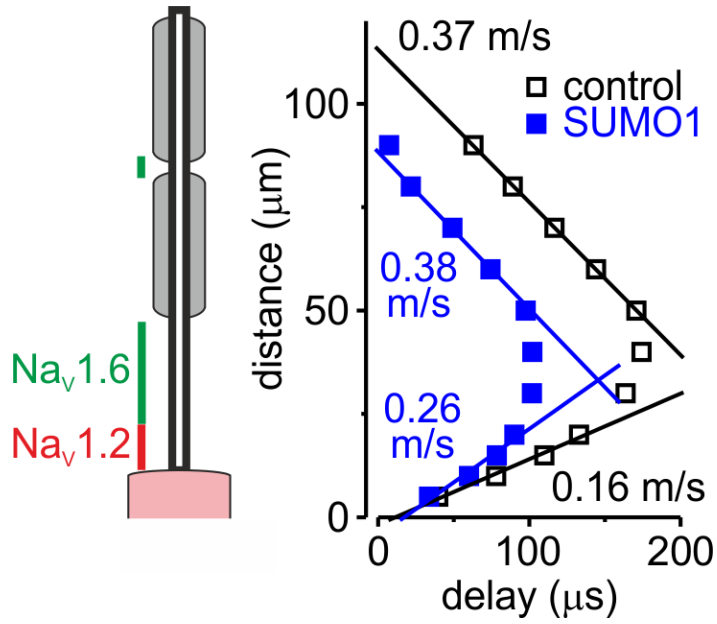

Figure 6 - Figure Supplement 1. In computational models, SUMOylation of $Na_v1.2$ channels selectively accelerates spike backpropagation.

Left, Schematic drawing of L5 pyramidal neuron with $Na_v1.2$ (red) present in the soma and proximal AIS and $Na_v1.6$ (green) localized in the distal AIS and nodes of Ranvier. *Right*, the delays of AP initiation plotted against distance from the edge of the soma in the model of a neuron under control conditions (black) and following the SUMO1 dialysis. Straight lines are linear fits of the linear portions of the delay-distance relationship with their slopes representing the velocities of back- and forward-propagation velocities. Note that SUMOylation of $Na_v1.2$ channels selectively enhances the velocity of backpropagating AP.

831 **Supplementary Figures**

832

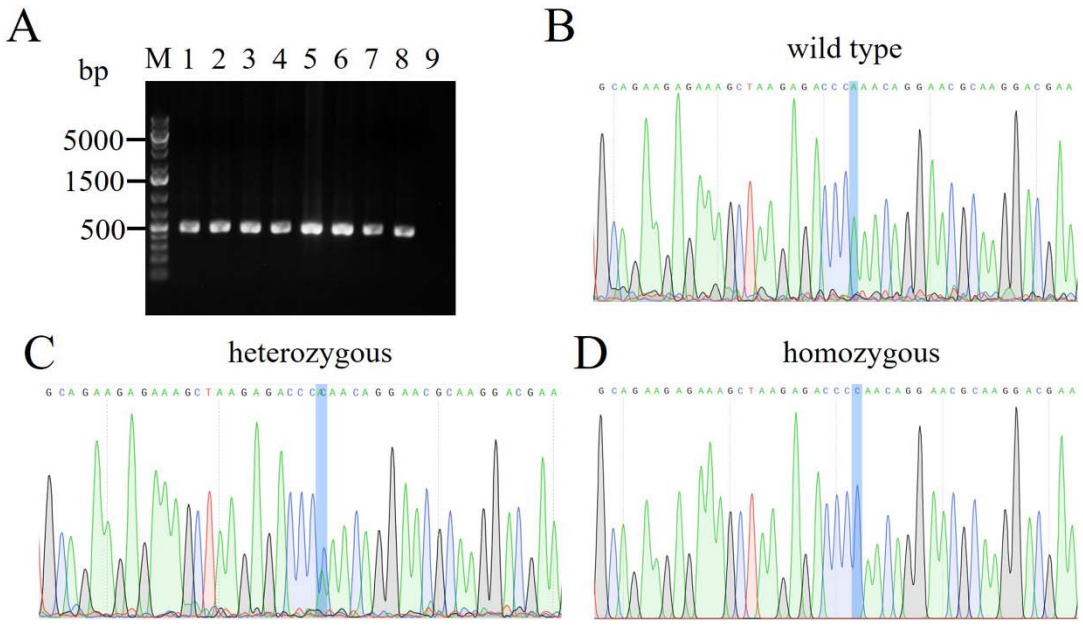

833

834 **Figure S1**. Genotyping of transgenic mice obtained through CRISPR-Cas9 targeting of
835 the *Scn2a* gene.

836 (A) PCR screening. Results of 8 pups are shown (lanes 1-8). The CRISP-targeted *Scn2a*
837 locus was amplified from genomic DNA isolated from mouse tails using two gene-
838 specific primers (*Scn2a*-F: 5'-CCGCCAGGACCTGACAGCTTC-3';π *Scn2a*-R: 5'-
839 CATGCCCCCTTGCAGGATGCC-3'). The PCR products were separated by gel
840 electrophoresis on a 2% agarose gel. The expected amplicon size is 457 bp for all wide
841 type, heterozygous and homozygous samples. No band was observed in the non-template
842 control (lane 9).

843 (B) Representative sequencing of PCR amplicon of the wide-type sample. Lys38,
844 encoded by the AAA codon, was shown in the wild-type allele.

(C) Representative sequencing of PCR amplicon of the heterozygous sample. Double peaks of A and C nucleotides evidenced the integration of the Lys38Gln mutation in the genome (Codon AAA = Lysine → CAA = Glutamine).

(D) Representative sequencing of PCR amplicon of the homozygous sample. Glutamine, encoded by the CAA codon, confirmed the replacement of Lys38 in the genome.